

HCO⁺ OBSERVATIONS TOWARD COMET HALE-BOPP (C/1995 O1): ION-MOLECULE CHEMISTRY AND EVIDENCE FOR A VOLATILE SECONDARY SOURCE

S. N. MILAM, C. SAVAGE, AND L. M. ZIURYS

Department of Chemistry, Department of Astronomy, and Steward Observatory, 933 North Cherry Avenue,
University of Arizona, Tucson, AZ 85721

AND

S. WYCKOFF

Department of Physics and Astronomy, Arizona State University, Tempe, AZ 85287

Received 2004 February 20; accepted 2004 July 19

ABSTRACT

Several millimeter-wave transitions of HCO⁺ have been detected toward comet Hale-Bopp (C/1995 O1) using the Arizona Radio Observatory 12 m telescope. The $J = 2 \rightarrow 1$ transition at 178 GHz was observed toward the comet nucleus near perihelion on 1997 March 10 and 20, as well as the $J = 3 \rightarrow 2$ transition at 268 GHz on 1997 March 9, with angular resolutions of 36'' and 23'', respectively. These data all show a slight velocity shift (~ 1.2 km s⁻¹) from the nominal comet velocity, and the $J = 3 \rightarrow 2$ profile is asymmetric with a redshifted wing. These differences likely arise from ion acceleration by the solar wind. A rotational diagram analysis of the data yielded a column density of 1.1×10^{12} cm⁻² for HCO⁺ in Hale-Bopp, which corresponds to an average number density of 36 cm⁻³. The data taken on March 9 show a second velocity component redshifted by 7.0 ± 0.6 km s⁻¹, which is considerably weaker than the main feature and appears to have a counterpart in the HNC, $J = 3 \rightarrow 2$ data, observed within an hour of the HCO⁺ measurements. The velocity difference between the main and secondary emission lines deprojected onto the extended solar radius vector is ~ 10 km s⁻¹ for both HCO⁺ and HNC, and the weak-to-strong line intensity ratios ($\sim 5\%$) are identical to within observational errors, suggesting a common high-velocity volatile secondary source. A plausible model that may account for the redshifted velocity components is a comoving, localized debris field of submicron refractory grains accelerated by solar radiation pressure located $\sim 10^5$ – 10^6 km from the nucleus. The parent material of the weaker redshifted HNC and HCO⁺ lines may be predominately complex organic polymers. An examination of the production rates for HCO⁺ suggests that the reaction $\text{H}_2 + \text{CO}^+$ is likely to be an important route to this ion in the outer coma beyond the collisionopause, where it has its peak abundance.

Subject headings: astrochemistry — comets: individual (Hale-Bopp (C/1995 O1)) — line: profiles — molecular data — radio lines: solar system — solar wind

1. INTRODUCTION

Comets are thought to contain pristine material relatively well preserved from the early solar system. These objects were probably created in the outer presolar nebula and therefore document the chemical history of this era and that of the protoplanetary disk. Whipple's (1950) "dirty snowball" model with a small solid nucleus of refractory material mixed with ices and other frozen matter has been well substantiated by observations of many comets (e.g., Crovisier & Encrenaz 2000). As a comet approaches the Sun, a small amount of the frozen material sublimates to form an expanding coma of gas and dust. A small fraction of the coma gas is photoionized, some of which is accelerated in the antisolar direction to form the plasma tail.

Because of its extreme brightness, comet C/1995 O1 (Hale-Bopp) was one of the most extensively observed comets. At 7 AU, this object was already 100 times brighter than comet Halley, with a visual magnitude of 11 (e.g., Crovisier & Encrenaz 2000). The comet was observed at multiple wavelengths, including IR, UV, visible, X-ray, and radio (e.g., Dello Russo et al. 2000; Owens et al. 1999; Lis et al. 1999; Lovell et al. 1998; Ziurys et al. 1999). Because it has a long period and a highly inclined orbit, Hale-Bopp most likely arises from the Oort Cloud.

With the appearance of Hale-Bopp, the inventory of known chemical compounds in comets tripled (Bockelée-Morvan et al. 2000), including the addition of several new molecular ions. Investigating ions is important because they help to establish physical and chemical processes in the coma, as well as comet-solar wind interactions. The latter effect in fact causes a small acceleration (~ 1 – 10 cm s⁻²) of the ions in the antisolar direction that has been observed in many comets, including Hale-Bopp (e.g., Lovell et al. 1998; Crovisier & Bockelée-Morvan 1999). Because the species frozen in the cometary ice are likely to only be neutrals, ions must form from sublimated gas by some combination of photoionization, charge exchange, electron impact, and ion-molecule reactions in the comet coma (Crovisier & Encrenaz 2000).

HCO⁺ is an ion of particular interest for cometary studies. Although this species is fairly ubiquitous in molecular clouds, it has only recently been observed in comets. The first detection of HCO⁺ occurred in Hale-Bopp in 1997 February, where the $J = 1 \rightarrow 0$ transition at 89 GHz was measured using the BIMA antennas in autocorrelator mode (Veal et al. 1997). Other rotational transitions were subsequently observed, including the $J = 3 \rightarrow 2$ and $J = 4 \rightarrow 3$ lines at 268 and 357 GHz, respectively, using the Submillimeter Telescope (SMT) on March 5 and 9 (Narayanan et al. 1997). Lis et al. (1999) also detected the $J = 3 \rightarrow 2$ transition on March 26 using the Caltech

Submillimeter Observatory telescope. All millimeter detections occurred within a 5 month period, when the comet was brightest, from 1997 January to May, with most observations conducted from February to March.

In addition to spectral line detections, the spatial distribution of HCO⁺ was also measured in Hale-Bopp. Lovell et al. (1998, 1999), for example, mapped the $J = 1 \rightarrow 0$ transition of this ion in the comet using the Five College Radio Astronomy Observatory (FCRAO) 14 m antenna during the period of March 21 to April 27. These authors discovered a local emission minimum centered on the nominal position of the comet nucleus on several dates, as well as an asymmetric ring around the nucleus with a strong anti-sunward peak. The HCO⁺ emission region also proved to be time variable and quite extended; the species was detected 50,000–300,000 km from the nucleus. Furthermore, during March, Womack et al. (1999) mapped the $J = 1 \rightarrow 0$ line using the NRAO 12 m telescope using the on-the-fly technique and found a similar “void” at the nucleus in HCO⁺ emission. These authors explained the void as arising in the “diamagnetic cavity” where low electron temperatures in this magnetic field-free region increased the ion dissociative recombination rate and hence the destruction of HCO⁺ and other ions. Wright et al. (1998) also published mosaicked images and spectra on the $J = 1 \rightarrow 0$ transition of HCO⁺, using the BIMA interferometer. This map does not show a void near the nucleus on May 6, providing further evidence of the variability of the HCO⁺ distribution.

The unusual and time-variable distribution of ions such as HCO⁺ in Hale-Bopp, as well as recent studies of other bright comets, clearly requires a coma source more complex than Whipple’s (1950) single-source nucleus model. In situ *Giotto* spacecraft data collected from the coma of comet Halley, for example, indicated that about half of the CO and virtually all of the H₂CO were both slowly released from a distributed source extending $\sim 10^4$ km from the nucleus and likely attributable to long-lived small organic particles composed mostly of the elements carbon, hydrogen, oxygen, and nitrogen (CHON; Eberhardt 1999). Dust coma sources, accounting for about half of the CO and CN and virtually all of the H₂CO, have been reported for several comets (A’Hearn et al. 1986; Wink et al. 1999; Disanti et al. 1999). Additional evidence for extended circumnuclear source regions comes from jets spatially offset from the nucleus, as well as coma knots, condensations, and arclets, all indicative of secondary coma source regions in the form of fragments co-orbiting or released from the comet nuclei (Harris et al. 1997; Desvoivres et al. 1999; Blake et al. 1999; Gunnarsson et al. 2003).

Puzzling parallel bands (striae) observed in dust tails of many bright comets have been attributed to the disintegration of fragments of long-lived friable material located far ($>10^6$ km) from the comet nucleus (Sekanina & Farrell 1980). Striae are possibly related to interplanetary dust particles (e.g., Arpigny et al. 2003) and meteoritic material collected in the Earth’s atmosphere that have been identified as comet debris (e.g., Sekanina & Farrell 1980). The icy material comprising comet solids probably has a very low tensile strength (Whipple 1999), and a few percent of comet nuclei have split or entirely disintegrated (Sekanina 1982; Weaver et al. 2001; Boehnhardt 2002), apparently as a consequence of their low tensile strengths, not tidal interactions with planets or the Sun. Hence a picture is emerging of a friable water ice-dominated comet nucleus surrounded by circumnuclear icy fragments with size scales ranging from submicron to tens of meters that slowly degrade into successively smaller, refractory-rich fragments (<2 AU).

The refractory debris contributes to the expanding coma and further thermally degrades over long timescales ($\sim 10^5$ – 10^6 s; Sekanina & Farrell 1980) into complex organic parent molecules of the observed HNC, CO, and H₂CO (e.g., Sekanina & Farrell 1980; Huebner et al. 1987, 1991; Jewitt & Matthews 1999; Rodgers & Charnley 2001; Charnley et al. 2002; Cottin et al. 2001).

In this paper, we report independent detections of the $J = 2 \rightarrow 1$ and $J = 3 \rightarrow 2$ transitions of HCO⁺ toward the comet, using the Kitt Peak 12 m telescope. The $J = 2 \rightarrow 1$ transition had not been previously observed. From these spectra, a column density and rotational temperature were determined. In addition to a broad, redward Doppler-shifted wing, a weak high-velocity (~ 7 km s⁻¹) component appears in the HCO⁺ spectra on March 9 that has a counterpart in the HNC spectrum observed on the same day. Here we suggest that these weak line components may have arisen from a transient secondary coma source created when a coma fragment abruptly disintegrated into a debris field rich in organic grains, such as CHON particles or complex organic polymers (Huebner et al. 1991; Rogers & Charnley 2001; Cottin et al. 2001). Submicron grains were then selectively accelerated by solar radiation pressure to ~ 10 km s⁻¹ on a timescale of ~ 1 – 2 days. In this scenario the weak, redshifted components of both HCO⁺ and HNC arose from thermal degradation of the accelerated debris field located roughly 10^5 – 10^6 km on the antisolar side of the nucleus.

2. OBSERVATIONS

Measurements of HCO⁺ were carried out during the period 1997 March 9 to March 20. The observations were made using the former NRAO 12 m telescope at Kitt Peak, Arizona.¹ The receivers used were dual-channel SIS mixers, operated in single-sideband mode with image rejection around 20 dB, covering the 2 and 1.2 mm bands. The back ends employed were filter banks with 250 kHz, 500 kHz, or 1 MHz resolution, depending on the given frequency. The temperature scale was determined by the chopper-wheel method and is given in terms of T_R^* , corrected for forward spillover losses (η_{fss}). Radiation temperature is then determined using η_c , the corrected beam efficiency, where $T_R = T_R^*/\eta_c$. The position of the comet was determined through a two-body ephemeris program using the orbital elements provided by D. Yeomans of JPL. The telescope was pointed toward the nominal ephemeris position of the nucleus and tracked at the comet’s predicted ephemeris rates during the observations. To ensure positional accuracy, periodic pointing and focusing on Jupiter and Saturn were conducted. Data were collected by position-switching with the off position 30’ west in azimuth.

Observing frequencies used for HCO⁺ are listed in Table 1. Also given are the beam efficiencies at these frequencies and the respective angular and linear beam sizes projected at the comet, as well as the comet’s heliocentric (R_h) and geocentric (Δ) distances.

3. RESULTS

Table 1 summarizes the observational results for HCO⁺. As the table shows, the $J = 2 \rightarrow 1$ line of HCO⁺ at 175 GHz was

¹ The National Radio Astronomy Observatory is a Facility of the National Science Foundation operated under cooperative agreement by the Associated Universities, Inc. The Kitt Peak 12 m telescope is currently operated by the Arizona Radio Observatory at Steward Observatory (the University of Arizona), with support from the Research Corporation.

TABLE 1
OBSERVATIONS AND ABUNDANCES TOWARD COMET HALE-BOPP

Molecule	Transition ($J+1 \rightarrow J$)	UT Date (1997)	ν (MHz)	θ_b (arcsec)	D (km)	η_c	T_R^* (K)	$\Delta v_{1/2}$ (km s^{-1})	R_h (AU)	Δ (AU)	N_{tot} (cm^{-2})
HCO ⁺	3 \rightarrow 2	Mar 9.95	267,557.6	23	23,640	0.42	0.52 \pm 0.01	3.5 \pm 0.3	1.003	1.387	1.08 \times 10 ^{12a}
	0.08 \pm 0.03 ^b	1.5 \pm 1.2 ^b
	2 \rightarrow 1	Mar 10.59	178,375.1	36	35,950	0.67	0.51 \pm 0.09	3.7 \pm 0.6	0.996	1.377	1.08 \times 10 ^{12a}
	2 \rightarrow 1	Mar 20.63	178,375.1	36	34,410	0.67	0.45 \pm 0.04	3.3 \pm 0.3	0.940	1.318	4.31 \times 10 ^{11c}
HNC ^d	3 \rightarrow 2	Mar 9.92	271,981.1	23	23,184	0.38	0.66 \pm 0.05	2.3 \pm 0.3	1.003	1.387	3.4 \times 10 ¹²
	0.08 \pm 0.03 ^b	1.1 \pm 0.9 ^b

NOTE.—Errors are 3 σ .

^a N_{tot} derived from rotational diagram (see text).

^b The second component redward of the main line in Fig. 1.

^c Assumes $T_{\text{rot}} = 7$ K.

^d From Ziurys et al. (1999).

observed on the UT dates March 10 and March 20. The $J = 3 \rightarrow 2$ transition of HCO⁺ at 267 GHz and the $J = 3 \rightarrow 2$ transition of HNC at 272 GHz were measured on March 9 only. Line parameters are also given in this table, which were determined by fitting Gaussians to the line profiles of each of the spectra. As the table shows, the HCO⁺ spectra typically had $T_R^* \sim 0.5$ K and line widths near 3.5 km s^{-1} . These line widths are somewhat broader than typically observed in comets for neutral molecules. For example, HCN had a line width of 2.3 km s^{-1} in the $J = 3 \rightarrow 2$ transition in comet Hale-Bopp (Ziurys et al. 1999).

Spectra obtained from comet Hale-Bopp are presented for each date observed in Figures 1 and 2. Figure 1 displays the spectra of the $J = 3 \rightarrow 2$ transition of HCO⁺ (integration time 48 minutes) and the $J = 3 \rightarrow 2$ transition of HNC (integration time 1 hr), both recorded on March 9. Figure 2 displays the $J = 2 \rightarrow 1$ transition of HCO⁺ on March 10 (integration time 1 hr 48 minutes) and March 20 (with 1 hr integration time). All figures are plotted in the cometocentric velocity frame. Each HCO⁺ transition displays a strong central peak shifted by ~ 1.2 km s^{-1} from the predicted geocentric comet velocity (cf. HNC velocity in Fig. 1). Also, the $J = 3 \rightarrow 2$ line of HCO⁺ shows an asymmetric profile with a redshifted tail, which is in the antisolar direction. This effect has been seen in other ion spectra (Lovell et al. 1998; Wright et al. 1998; Womack et al.

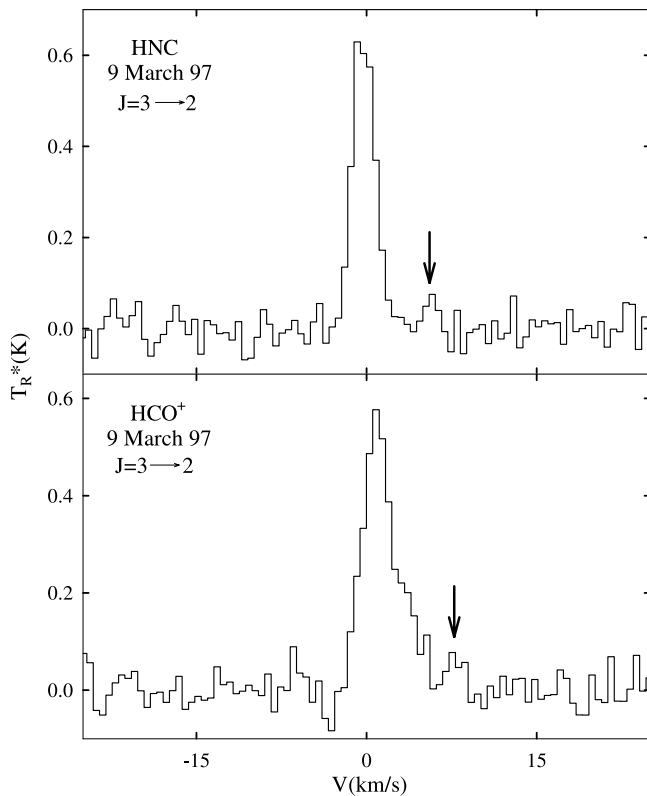


FIG. 1.—The $J = 3 \rightarrow 2$ transition of HCO⁺ at 268 GHz and the $J = 3 \rightarrow 2$ line of HNC at 272 GHz detected toward comet Hale-Bopp, using the 12 m telescope on 1997 March 9 with 500 kHz (0.55 km s^{-1}) resolution. A second velocity component appears to be present in both spectra, shifted by about 5 km s^{-1} from the main line, indicated by arrows. The HNC feature is at the nominal comet velocity, while that of HCO⁺ is redshifted by $\sim 1.2 \text{ km s}^{-1}$. The HCO⁺ profile also is asymmetric with a prominent redshifted line wing. Spectra are plotted in a cometocentric velocity frame.

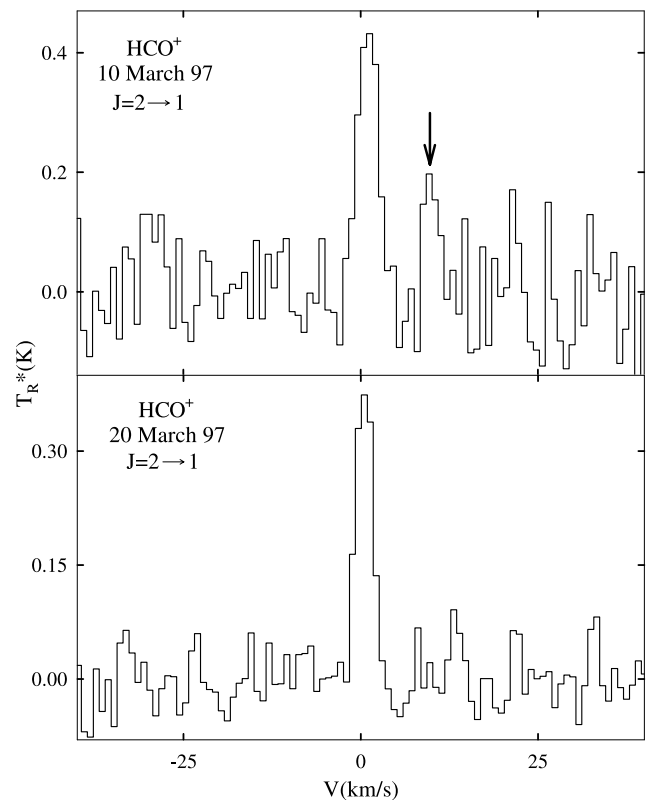


FIG. 2.—The $J = 2 \rightarrow 1$ transition of HCO⁺ at 178 GHz detected on 1997 March 10 and 20 toward comet Hale-Bopp, using 500 kHz resolution. A second component may be present in the March 10 data, as indicated by an arrow, but is not visible in the March 20 spectrum.

1999; Narayanan et al. 1997). The slight redward displacement and asymmetry likely arise from the antisolar motional force due to the solar wind interaction with the comet. Lovell et al. (1999) estimated the HCO⁺ acceleration to be $\sim 10 \text{ cm s}^{-2}$ in 1997 March.

In addition to the main emission-line feature, both the HNC and the HCO⁺ ($J = 3 \rightarrow 2$ and $J = 2 \rightarrow 1$) lines have weaker redshifted velocity components, displaced from the stronger lines by $\sim 7 \text{ km s}^{-1}$ (indicated by arrows in Figs. 1 and 2). These redshifted velocity components do not arise from extraneous background sources, nor are they likely caused by interaction with the solar wind, since the neutral (HNC) and ionic (HCO⁺) species both display the same velocity shifts and have similar primary-to-secondary intensity ratios. If associated with the comet, these redshifted velocity components may represent the first spectroscopic evidence for a distinct secondary coma source rich in volatile complex organic compounds. If so, the relatively high velocity can probably be explained by solar radiation pressure forces acting on submicron-sized grains rich in organic material. The velocities for the HNC and HCO⁺ line pairs associated with the secondary source, deprojected onto the solar radius vector, $v_{ss} \approx 10 \text{ km s}^{-1}$, are well in excess of the escape velocity from the comet nucleus, $v_{esc} \approx 15 \text{ m s}^{-1}$ (radius $r_n \sim 20 \text{ km}$). If the weak HCO⁺ component indicated in Figure 2 (*top*) is real, its deprojected velocity is $\sim 13 \text{ km s}^{-1}$, corresponding to an acceleration of the secondary source $a_{ss} \sim 0.05 \text{ m s}^{-2}$. This acceleration would require an antisolar force about 10 times the solar gravitational attraction.

4. ANALYSIS

4.1. Abundances of HCO⁺

Since the projected beam diameters of the 12 m telescope (see Fig. 3 and Table 1) at both observing frequencies are smaller than the collisionopause, it is most probable that the excitation of HCO⁺ is dominated by collisions with H₂O. The collisionopause of a comet is defined by the mean free path of a neutral molecule in a water-dominated coma (e.g., Wyckoff 1982). For Hale-Bopp, with $Q(\text{H}_2\text{O}) \sim 10^{31} \text{ molecules s}^{-1}$ and an outflow velocity of $v \sim 1 \text{ km s}^{-1}$, the mean free path is $\sim 8 \times 10^4 \text{ km}$ for an assumed neutral-neutral collisional cross section of $\sigma \sim 10^{-15} \text{ cm}^2$ or a collisionopause of $r \sim 10^5 \text{ km}$ centered at the nucleus. The only other form of excitation is by solar radiation as the comet approaches perihelion, which can be estimated for comparison. This radiative rate g is defined as $g = (\pi e^2 / mc^2) f F_{\odot}$, where $\pi e^2 / mc^2 = 8.82 \times 10^{-13} \text{ cm}$, f is the absorption oscillator strength, and F_{\odot} is the solar flux (Weaver & Mumma 1984). Using this formula, g is calculated to be $\sim 10^{-6} \text{ s}^{-1}$ for HCO⁺. In contrast, the collision rate (with water) for excitation from the $J = 2$ level to the $J = 3$ level is $\sim 2 \times 10^{-5} \text{ s}^{-1}$, assuming a cross section of $\sigma = 10^{-14} \text{ cm}^2$ (Crovisier 1987), a density of $n_{\text{H}_2\text{O}} = 1.2 \times 10^5 \text{ cm}^{-3}$ (Dello Russo et al. 2000), and a kinetic temperature of 50 K. This value is significantly faster than the radiative rate.

Because collisional excitation is dominant, a rotational diagram was constructed to estimate the column density of HCO⁺. In such diagrams, the slope is inversely related to the rotational temperature T_{rot} and the y -intercept establishes the total column density, assuming that the gas is optically thin and in thermal equilibrium. Four data points were included in this analysis: the $J = 3 \rightarrow 2$ and $J = 2 \rightarrow 1$ transitions [$E_{\text{rot}}(J) = 12.84$ and 8.56 K] from this work and the $J = 3 \rightarrow 2$ and $J = 4 \rightarrow 3$ ($E_{\text{rot}} = 17.12 \text{ K}$) lines from the SMT observations

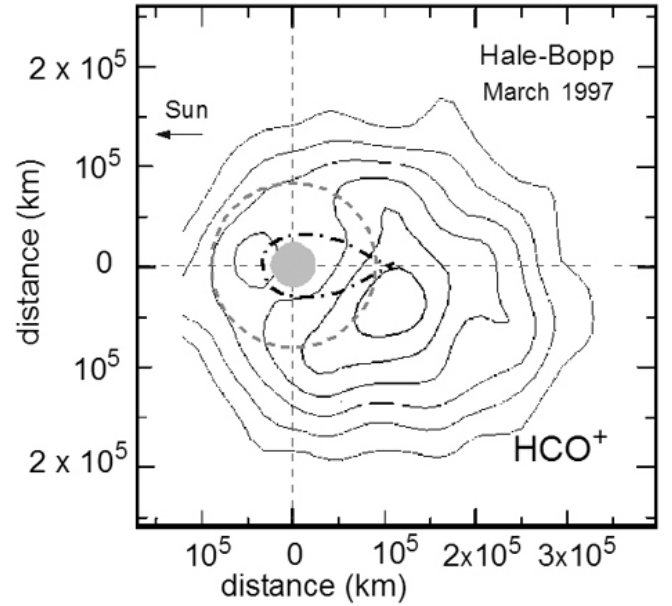


FIG. 3.—HCO⁺ emission distribution (isophotes adapted from Lovell et al. 1999) in comet Hale-Bopp. Projected beam size of 12 m telescope for $J = 2 \rightarrow 1$ transition, centered on nominal position of comet nucleus at position (0, 0), is indicated by the gray circle. Within the magnetic field-free ionopause (dot-dashed line; also called the diamagnetic cavity), HCO⁺ ions initially expand with neutrals at 1 km s^{-1} . Ion-molecule chemical reactions produce HCO⁺ over an extended region; a significant fraction is observed outside the collisionopause (dashed circle with radius 80,000 km). The low intensity of HCO⁺ emission in the ionopause and the collisionopause regions is likely due to rapid destruction of these ions by dissociative recombination.

(Narayanan et al. 1997). These HCO⁺ lines were all detected at approximately the same heliocentric distance (March 5 through March 10). The equation used to determine an average HCO⁺ column density for these dates is

$$\log(3kT_R \Delta v_{1/2} / 8\pi^3 \nu S_{ij} \mu_0^2) = \log(N_{\text{tot}} / g_{\text{rot}}) - (\log e)(E_u / T_{\text{rot}}), \quad (1)$$

where ν is the frequency, S_{ij} is the line strength, μ_0 is the permanent dipole moment (4.0 D), g_{rot} is the rotational partition function, and N_{tot} is the total number of HCO⁺ ions observed in the beam.

The results of this analysis are shown in Figure 4. The data taken with the 12 m are shown by filled circles and that from the SMT by unfilled circles. As is apparent in Figure 4, the $J = 3 \rightarrow 2$ column density obtained with the 12 m telescope is consistent with the observations obtained with the SMT (Narayanan et al. 1997), and all four data points lie along a straight line, lending credibility to this analysis. The rotational temperature derived from the plot in Figure 4 is approximately 7 K, and the total column density is $N_{\text{tot}} = 1.1 \times 10^{12} \text{ cm}^{-2}$. This value is in close agreement with those reported by other authors. For example, Narayanan et al. (1997) estimated a column density from the $J = 3 \rightarrow 2$ and the $J = 4 \rightarrow 3$ transitions of $2.7 \times 10^{12} \text{ cm}^{-2}$. The column density reported here corresponds to a space density of 36 cm^{-3} , given a region with a radius of $r \sim 1.5 \times 10^{10} \text{ cm}$ (Lovell et al. 1999).

The $J = 2 \rightarrow 1$ line was also observed separately on March 20. To calculate a total column density on this date, the following formula was used, which assumes low optical depth:

$$N_{\text{tot}} = (3kT_R \Delta v_{1/2} / 8\pi^3 \nu S_{ij} \mu_0^2) g_{\text{rot}} / e^{-\Delta E / kT_{\text{rot}}}. \quad (2)$$

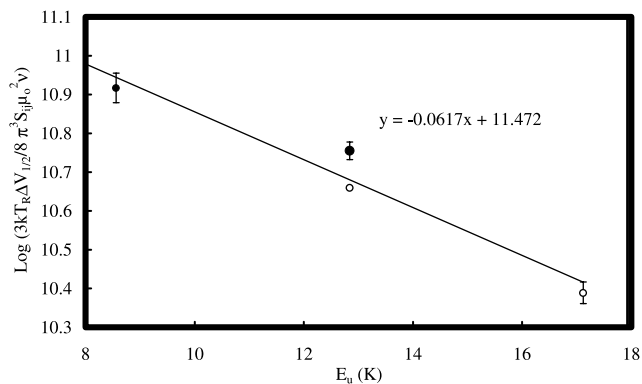


FIG. 4.—Rotational diagram for HCO^+ in comet Hale-Bopp (1997 March). Filled circles: Data presented from this study. Open circles: Data from Narayanan et al. (1997). The diagram indicates $N_{\text{tot}} = 1.1 \times 10^{12} \text{ cm}^{-2}$ and $T_{\text{rot}} = 7 \text{ K}$ for HCO^+ .

The symbols have identical meaning as in equation (1), and ΔE indicates the energy of the $J = 2$ level above ground state. A rotational temperature of 7 K was used, as indicated by the rotational diagram. The resulting column density for March 20 was calculated to be $N = 4.3 \times 10^{11} \text{ cm}^{-2}$, about a factor of 3 lower.

These equations, however, assume the Rayleigh-Jean limit, namely, $h\nu \ll kT_{\text{ex}}$, which may not be appropriate. For comparison, a column density was also calculated from the $J = 2 \rightarrow 1$ data without the Rayleigh-Jean approximation; $N_{\text{tot}} = 4.647 \times 10^{11} \text{ cm}^{-2}$ was derived. The two values differ by only 8%, and hence the former assumption is justified.

4.2. Chemical Schemes for HCO^+ Production and Destruction

The only plausible mechanism for creating HCO^+ in this very high production rate comet is by chemical reactions in the coma (e.g., Lovell et al. 1998, 1999; Irvine et al. 1998). Three reactions are possible for HCO^+ synthesis in the coma:

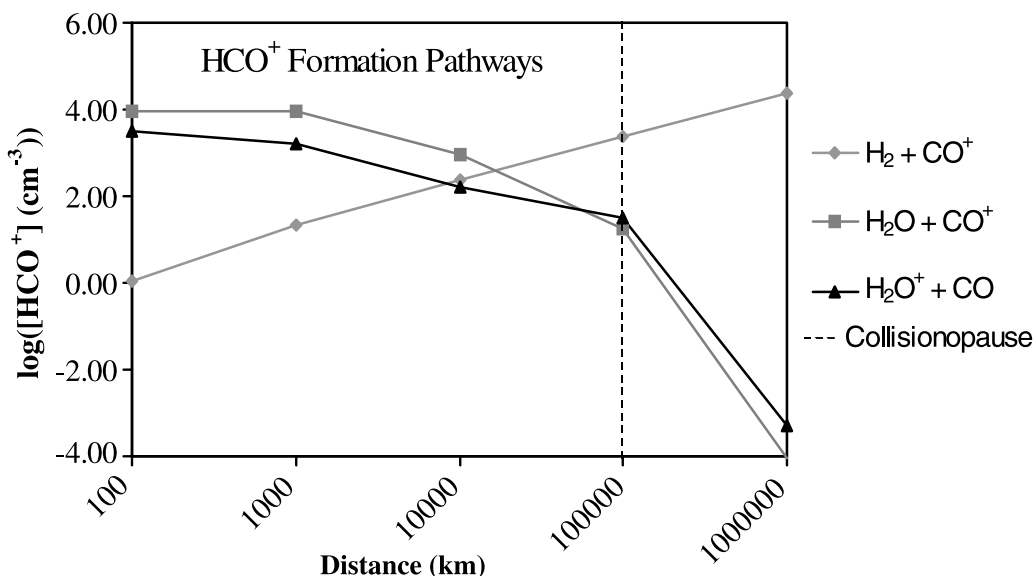
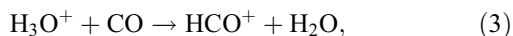
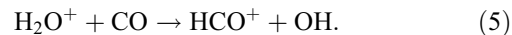
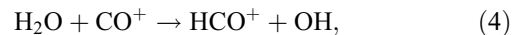
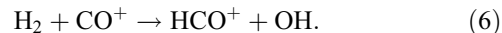


FIG. 5.—Plot illustrating the relative importance of the reactions $\text{H}_2\text{O}^+ + \text{CO}$, $\text{H}_2\text{O} + \text{CO}^+$, and $\text{CO}^+ + \text{H}_2$ in the production of HCO^+ . Inside the collisionopause (indicated by the dashed line at 10^5 km), water and H_2O^+ are the major precursors. However, near the edge of this region, the H_2 abundance has sufficiently risen to enable the pathway $\text{H}_2 + \text{CO}^+$ to dominate HCO^+ synthesis.



Reaction (4) cannot be significant because H_2O has a higher proton affinity than CO (Huntress et al. 1980). Irvine et al. (1998) suggest that reaction (5) is the likely source of HCO^+ , which is consistent with the broad distribution of CO^+ predicted by models (Gombosi et al. 1999). The rate of this reaction is $k_5 = 8.8 \times 10^{-10} \text{ cm}^3 \text{ s}^{-1}$ (Le Teuff et al. 2000). The model by Gombosi et al. (1999) also predicts large abundances of H_2O^+ at the nucleus and throughout the comet tail. Given the high relative abundance of CO within the collisionopause in Hale-Bopp, reaction (6) is also a viable route to HCO^+ . This reaction has a rate of $k_6 = 5.0 \times 10^{-10} \text{ cm}^3 \text{ s}^{-1}$, which is comparable to that of reaction (5).

On the other hand, H_2O is rapidly destroyed by photodissociation within the collisionopause as predicted, for example, by the model of Lovell et al. (1999). The photodissociation of water leads mainly to H , OH , and O , but H_2 and H_2O^+ are also significant products (Huebner et al. 1992). Because a large amount of CO^+ exists beyond the collisionopause, another way to produce HCO^+ is



This reaction proceeds at a rate of $k_6 = 1.8 \times 10^{-9} \text{ cm}^3 \text{ s}^{-1}$ (Le Teuff et al. 2000), which is certainly competitive with the other HCO^+ formation rates.

A quantitative comparison of these three major production schemes of HCO^+ is illustrated by Figure 5, which displays the density of HCO^+ (in cm^{-3}) as a function of distance from the nucleus, calculated separately from reactions (5), (6), and (7). The density of water, CO , and CO^+ used in the computations was taken from Lovell et al. (1999), and that of H_2O^+ from Gombosi et al. (1999). To determine the density of H_2 , the branching ratios for the photodestruction of water by Huebner et al. (1992) were used (an average density of $\sim 10^6 \text{ cm}^{-3}$ was obtained). An outflow velocity of 1 km s^{-1} was also assumed. Figure 5 clearly shows that the reactions starting with H_2O and

H₂O⁺ are the dominant source of HCO⁺ within the collision-pause ($r_N \sim 1 \times 10^5$ km), but they become insignificant compared to the H₂ reaction outside of that region.

HCO⁺ is likely destroyed by photodissociation, proton transfer to H₂O, and dissociative electron recombination. Using the cross section of Koch et al. (1995), the photodissociation rate for HCO⁺ ($R = 1$ AU) is 4.18×10^{-8} ions s⁻¹, which corresponds to a lifetime of $\tau \sim 2.4 \times 10^7$ s or 277 days. Proton transfer via the reaction $\text{H}_2\text{O} + \text{HCO}^+ \rightarrow \text{CO} + \text{H}_3\text{O}^+$ has a rate of 2.5×10^{-9} cm³ s⁻¹ (Le Teuff et al. 2000). Assuming that the HCO⁺ density is 36 cm⁻³, the lifetime for HCO⁺ with destruction by this reaction is $\tau \sim 1 \times 10^7$ s, or 129 days. In contrast, at 50 K, the electron recombination rate was calculated to be 5.22×10^{-8} cm³ s⁻¹ (Le Teuff et al. 2000). From the model of Lovell et al. (1999), the electron density falls in the range $n_e \sim 10^3$ – 10^5 cm⁻³ over the region traced by HCO⁺ (see Fig. 3). Therefore, the electron recombination rate for HCO⁺ is typically $\sim 5 \times 10^{-5}$ to 5×10^{-3} s⁻¹. Thus, the lifetime of this ion against dissociative electron recombination is about 3–300 minutes, making this pathway the primary destruction route by many orders of magnitude. This calculation also indicates that HCO⁺ is short lived and is likely formed in situ in the various cometary regions.

4.3. Origin of HNC and HCO⁺ in the High-Velocity Component

The stronger components in HNC and HCO⁺ (Figs. 1 and 2) arise from the nucleus region, since the line positions correspond to the nominal comet ephemeris positions, taking into account the solar wind-induced ion acceleration. The similar line intensity ratios of the two weaker components for HNC and HCO⁺, together with their identical redshifts relative to the main feature, constitute strong evidence that these lines are associated with a common secondary source. This redshifted coma component had not previously been reported for any comet, although other HCO⁺ spectra (e.g., Lovell et al. 1998; Lis et al. 1999) show a possible feature near 5 km s⁻¹ at about the same epoch. The main HCO⁺ and HNC lines (Fig. 1) have relatively high signal-to-noise ratios (~ 26), but for the weaker feature the ratio is about 3. The secondary source is not obvious in the March 20 spectra of HCO⁺ but may be present in the March 10 data (see Fig. 2), as noted above. No secondary velocity component was observed in HCN spectra, but this absence may be explained by masking of the hyperfine structure.

HNC, CO, and H₂CO are thought to be produced at least in part in the extended coma, not only the comet nucleus (Huebner et al. 1991; Cottin et al. 2001; Rodgers & Charnley 2001). For example, the map of HCN by Veal et al. (2000) on March 8 showed a nucleus-centered distribution extending $\sim 10^4$ km from the nucleus. In contrast, observations of HNC by Hirota et al. (1999) show a slightly more extended region than HCN (50'' vs. 38'', respectively). Blake et al. (1999) found that HCN and HNC arose from two distinct regions, leading to the suggestion that HNC arose from photodestruction of complex organic species or CHON particles when the comet was near the Sun, $R_h \sim 1$ AU (Rodgers & Charnley 1998; Rodgers et al. 2003).

As is the case for HNC, HCO⁺ is not a direct sublimation product. The primary component of HCO⁺ is probably created by ion-molecule reactions requiring an environment with significant collisional rates. Using the modeled number densities of Lovell et al. (1999), the ion-molecule reaction timescales in the ringlike region where HCO⁺ had peak abundances (Fig. 3 and Lovell et al. 1999) ranged from $\tau_{\text{im}} \sim 100$ s at a distance

from the nucleus $R_n \sim 10^3$ km to $\tau_{\text{im}} \sim 10^5$ s at $R_n \sim 10^5$ km. Consequently there is little question that most of the HCO⁺ was produced by ion-molecule reactions (and destroyed by electron recombination) in the dense inner coma. However, the high-velocity redshifted component of HCO⁺ may have been created in the same transient secondary source, which produced the HNC and presumably also made CO. Virtually all ($\sim 95\%$) of the H₂CO in Hale-Bopp arose from an extended coma source (Wink et al. 1999), perhaps from a formaldehyde polymer such as polyoxymethylene (POM; Huebner et al. 1991; Cottin et al. 2001). Destruction of POM material could also lead to HCO⁺.

4.4. Acceleration Mechanisms

Several mechanisms could accelerate small fragments from the vicinity of the nucleus preferentially in the antisolar direction. Comet Hale-Bopp had one of the highest levels of gas production ever observed in a comet and displayed activity at optical wavelengths (transient emission enhancements) over a large range in heliocentric distance ($R_h \sim 7$ AU). The comet was particularly active during the weeks before March as it approached perihelion (1997 April 1). Frequent outbursts, arcs, and jets of dust, OH, C₂, and CN were reported from January to August (e.g., Lederer et al. 1999; McCarthy et al. 1999; Schwarz et al. 1999). Jetlike structures were also noticeable in the HCN and HNC maps (Veal et al. 2000; Blake et al. 1999).

The nucleus mass ($m_n \sim 10^{16}$ kg) and rotation ($P_{\text{rot}} \sim 11.3$ hr) (e.g., Jewitt & Matthews 1999) set constraints on the dynamics of ejected fragments. A large fragment ejected by rotation from the comet nucleus would leave with a velocity $v_{\text{rot}} = 2\pi r_n / P_{\text{rot}} \sim 3$ m s⁻¹, less than the escape velocity $v_{\text{esc}} \sim 15$ m s⁻¹ for a nucleus radius $r_n \sim 20$ km (Weaver & Lamy 1999; Jewitt & Matthews 1999). The maximum size r_g for a small fragment lifted from the nucleus surface by sublimating gases with velocity $v_{\text{ej}} \sim 1$ km s⁻¹ ($R_h \sim 1$ AU) and gas production rate $Q \sim 10^{31}$ molecules s⁻¹ may have been larger for Hale-Bopp than for most comets [$r_g(\text{max}) \sim 15$ cm] with a terminal velocity $v_t \sim 10$ m s⁻¹ (Harmon et al. 1999) because of the large gas production rate. Hence the combination of nucleus rotation plus gas drag could have ejected fragments with sizes ≤ 15 cm from the surface.

Large-grain production rates comparable to gas production rates have been inferred from detections of icy grain halos using radar techniques (Harmon et al. 1999). The large grains have centimeter size scales and have been observed surrounding several comet nuclei out to distances of $R_n \sim 10^2$ – 10^3 km (e.g., Harmon et al. 1999). Large-grain evaporation and fragmentation can explain spherical gas comae, distributed sources, and discrepancies between radar and radio-continuum observations (Harris et al. 1997; Jewitt & Matthews 1997; Harmon et al. 1999). To account for the HCO⁺ and HNC components comoving with a velocity ~ 10 km s⁻¹, we suggest a secondary source originating from the abrupt disintegration of a near-nucleus fragment initially drifting with a velocity ~ 10 m s⁻¹. Depending on the grain size distribution and ice content of the resulting debris field, the subfragments were subjected to a variety of antisolar-directed net forces, including sublimation recoil (dominant for the 1 mm to 1 cm sized “mini comets”), solar radiation pressure (dominant for the submicron grains), and electrostatic forces (dominant for grains < 0.1 μm ; Horanyi & Mendis 1991; Ip & Jorda 1998). For an observed acceleration $a_{\text{ss}} \sim 0.05$ m s⁻², the dust debris source was accelerated to 10 km s⁻¹ on timescales of days and was located on the antisolar side of the nucleus at a distance $R_n \sim 10^5$ – 10^6 km, coinciding with the observed locations of both HCO⁺

and HNC (Lovell et al. 1999; Wink et al. 1999; Blake et al. 1999).

Our observations set limits to the lifetime of the secondary source associated with the HCO⁺ and HNC high-velocity components. The time interval between the March 9 and the March 10 observations was ~ 15 hr, and no redshifted weak HCO⁺ line was observed in the March 20 spectrum. Therefore, the secondary source lifetime is set at $\tau_{ss} \sim 10^4$ – 10^6 s.

If a sublimation jet force biased in the antisolar direction accounted for part of the acceleration of large (centimeter sized) icy grain fragments associated with the secondary source of gas velocity (~ 10 km s⁻¹), their lifetimes had to exceed the destruction timescales from sublimation, fragmentation, and collisions. The sublimation lifetime for a 1 cm dirty ice grain is about 1 hr ($R_h \sim 1$ AU), and for pure ice ~ 1 day (Mukai 1986). For an icy grain moving away from the Sun because of a sublimation recoil force, the acceleration due to this jet effect is

$$a_j = v_{ej}(dm_g/dt)m_g^{-1}, \quad (7)$$

where v_{ej} is the gas ejection velocity and the grain mass is

$$m_g = 4\pi\rho_g r_g^3/3, \quad (8)$$

where ρ_g is the mean density. The mass-loss rate is then given by

$$(dm_g/dt) = 7.5 \times 10^{-4} r_g^2 \text{ kg s}^{-1}, \quad (9)$$

where a mass-loss rate per unit area $d\mu/dt = 1.2 \times 10^{-4}$ kg m⁻² s⁻¹ is assumed (Harmon et al. 1999). This gas mass-loss rate scaling is consistent with the Hale-Bopp nucleus gas mass-loss rate and with the mass-loss rates observed for centimeter-sized grains in other comets (Harmon et al. 1999). The solar gravitational acceleration at 1 AU is

$$a_s = GM_s d_h^{-2} \sim 5.9 \times 10^{-3} \text{ m s}^{-2}, \quad (10)$$

where G is the gravitational constant, M_s is the mass of the Sun, and d_h is the heliocentric distance. For a 1 cm ice grain with $v_{ej} \sim 1$ km s⁻¹ and $\rho_g \sim 300$ kg m⁻³, we find the net antisolar acceleration $a_{net} = a_j - a_s \sim 0.05$ m s⁻². Thus, the time required to accelerate a 1 cm grain by sublimation recoil to $v_{ss} \sim 10,000$ m s⁻¹ is

$$t_g \sim v_{ss}/2a_{net} \sim 1 \text{ day}. \quad (11)$$

This value is an order of magnitude longer than the sublimation lifetime for dirty ice (1 AU) but the same order as the lifetime for pure ice (Mukai 1986). Since the large grains surrounding comet nuclei probably arise from hierarchical fragmentation (e.g., Harris et al. 1997), the freshly exposed ices may have lifetimes longer than indicated by dirty ice models, possibly closer to those of pure ice. If it survives, the distance from the nucleus, R_n , reached by a 1 cm ice grain accelerated by a sublimation jet effect is

$$R_n \sim a_{net} t_g^2/2 \sim 10^5 \text{ km}. \quad (12)$$

This distance is comparable to the size of the collisionopause and within the region where ion-molecule chemistry is significant (see Fig. 4).

Although sublimation recoil may have contributed to the antisolar acceleration of small grains, their short sublimation

lifetimes require an additional acceleration mechanism to account for the observed redshifted HNC and HCO⁺ lines. We therefore suggest that rapid thermal decomposition (or possibly crystallization) of a fragment suddenly produced a swarm of organic-rich material with submicron size scales, such as CHON particles or organic-rich polymers. A swarm of such particles (parent material of the observed HNC and HCO⁺) could have been *selectively* accelerated (because of their grain sizes) to velocities of ~ 10 km s⁻¹ on timescales of days by solar radiation pressure and, possibly, electrostatic forces. If these submicron-sized refractory particles were volatile (e.g., DiSanti et al. 1999; Rodgers & Charnley 2001), they could have accounted for the secondary source giving rise to the redshifted HNC and HCO⁺ lines. Solar radiation pressure acceleration is given by

$$a_r = 3L_s Q_{pr} (16\pi d_h^2 c \rho_g r_g)^{-1}, \quad (13)$$

where L_s is the solar luminosity, Q_{pr} is the radiation interaction efficiency, and c is the velocity of light (e.g., Harris et al. 1997). For a grain with $r_g \sim 10^{-7}$ m at 1 AU, $\rho_g \sim 1000$ kg m⁻³, $L_s \sim 3.9 \times 10^{26}$ W, and $Q_{pr} \sim 1$, a_r is estimated to be ~ 0.03 m s⁻². For a dielectric grain such as olivine charged by solar UV radiation and the cometary plasma environment, the electrostatic acceleration a_e is ~ 0.03 m s⁻² for a grain with $r_g \sim 10^{-7}$ m at $d_h = 1$ AU (Horanyi & Mendis 1991). Thus a submicron-sized grain at 1 AU would require ~ 4 days to accelerate to a velocity of 10 km s⁻¹ by radiation pressure alone and would require ~ 2 days for a combination of radiation pressure and electrostatic acceleration, reaching distances on the antisolar side of the nucleus in the range $R_n \sim 10^5$ – 10^6 km. If the decomposition timescales of the parents of HNC and HCO⁺ were comparable to the time of flight of the putative submicron dust debris field, then the redshifted lines may be explained by such a scenario. We note that the 12 m telescope field of view projected at the comet distance was 24,000 and 36,000 km for the March 9 and 10 observations, respectively. Thus, the debris field could have been dispersed over a large area, yet represent an enhancement of HCO⁺ and HNC over the ambient coma.

5. DISCUSSION

5.1. A Model of HCO⁺ Formation in Comet Hale-Bopp

HCO⁺ emission in Hale-Bopp appears to be concentrated in a large shell-like region offset from the nominal comet nucleus position in the tailward direction ($r_N \sim 10^5$ km) and extending over several hundred thousand kilometers, as shown in Figure 3. This shell-like HCO⁺ distribution has density peaks in the sunward ($r_N \sim 5 \times 10^4$ km) and the antisolar ($r_N \sim 10^5$ km) directions. The sunward HCO⁺ peak may be caused by two effects: (1) a decrease in the HCO⁺ destruction rate (due to an increase in electron temperature beyond the collisionopause; e.g., Lovell et al. 1998), and (2) stagnation/reversal of the outward HCO⁺ outflow due to mass loading of the incoming solar wind plasma. Between the collisionopause ($r_c \sim 10^5$ km) and the bow shock ($r_N \sim 2 \times 10^6$ km) that has formed on the sunward side of the coma, mass loading of the incoming solar wind by the cometary pickup ions tends to decelerate and to redirect the coma ion outflow tailward (e.g., Gombosi et al. 1999). This ion stagnation and flow reversal enhances the column densities of ions on the sunward side of the coma (Lovell et al. 1998). A further enhancement of the ion densities would be expected from a sudden increase in electron temperature beyond the collisionopause, where the electrons are

no longer collisionally coupled to the ion and neutral outflow (e.g., Gombosi et al. 1999; Lovell et al. 1998). This sunward HCO⁺ peak may also be associated with the H₂O⁺ pileup region identified in comet Hale-Bopp (Bouchez et al. 1999). The HCO⁺ enhancement at $r_N \sim 10^5$ km tailward is probably caused by the focusing of the ion flow (Gombosi et al. 1999).

The distribution of HCO⁺ is beyond the outer boundaries of the collisionopause as well. The collisionopause is defined as the area where water is the main collisional partner; however, there are clearly other collisional partners (e.g., CO and H₂). The critical density for collisional excitation of HCO⁺ ($J = 1 \rightarrow 0$) is on the order of $\sim 10^6$ cm⁻³. For HCO⁺ ($J = 1 \rightarrow 0$) emission to be present, these densities must exist. They are certainly high enough to allow for significant collisions and to promote ion-molecule chemistry within the collisionopause.

For carbon monoxide and water, the overall coma abundance ratio was found to be $n(\text{CO})/n(\text{H}_2\text{O}) \sim 23\%$ (Bockelée-Morvan et al. 2000). The ion-molecule production rates of HCO⁺ for reactions (5) and (6) with this correlated abundance ratio give the production ratio of the two reactions as $Q_5/Q_6 \sim k_5 n(\text{H}_2\text{O})/k_6 n(\text{CO}) \sim 7.7$. Consequently, reaction (5) is probably the dominant pathway for producing HCO⁺ within the collisionopause of the comet coma. Once H₂O is destroyed, reaction (7) may become the dominant source, contributing to the extended region of HCO⁺ observed well beyond the collisionopause.

5.2. The High-Velocity Secondary Source

Split nuclei have occurred for a few percent of both short- and long-period comets, with roughly 40 events documented (Boehnhardt 2002). When near the Sun ($R_h < 2$ AU), individual fragments of split nuclei have well-defined comae and tails. The fragments of split nuclei generally fade away and disappear on rapid timescales (hours to weeks) or may survive many subsequent perihelion passages (e.g., Sekanina 1982; Weaver et al. 2001). Occasionally, but not always, cometary outbursts are correlated with observed fragmentation events. Only the splitting of the Sun-grazing comets and Shoemaker-Levy 9 have been attributed with any certainty to gravitational tidal disruption, and no correlation is evident between the occurrences of split nuclei and their perihelion distances. The disruption, splitting, and fragmentation of comet nuclei have been attributed to (1) gravitational tides by the Sun and planets, (2) subsurface sublimation, (3) rotation, (4) thermal stress, and (5) collisions (Ip 2003; Boehnhardt 2002; Sekanina & Chodas 2004). Evidence that comet nuclei are surrounded by debris fields with centimeter-sized fragments and larger has been mounting for years, culminating with observations of the bright comets Hyakutake (C/1996 B2) and Hale-Bopp (e.g., Harris et al. 1997; Sekanina 1998a, 1998b; Harmon et al. 1999).

The observed ratios of the secondary to the primary HNC and HCO⁺ integrated line intensities are

$$\int I(\text{HCO}^+)_{\text{ss}} / \int I(\text{HCO}^+)_{\text{ps}} = 0.063 \pm 0.026, \quad (14)$$

$$\int I(\text{HNC})_{\text{ss}} / \int I(\text{HNC})_{\text{ps}} = 0.054 \pm 0.032, \quad (15)$$

where the subscripts “ps” refer to the stronger HNC and HCO⁺ lines. As indicated by the HCO⁺ map in Figure 3, the observations on 1997 March 9 probed a line of sight in the 12 m field of view with diameter $\sim 10^4$ km (Table 1). The distribution of

HCO⁺ was shell-like, while the distribution of HNC was quite different at that time. Thus, the primary line components of these two species were averaged through quite different columns in the coma. We have argued that the secondary source producing the weaker lines of HNC and HCO⁺ was a localized region at a distance $R_n \sim 10^5$ – 10^6 km. Thus, it is quite remarkable that the ratios in equations (14) and (15) were roughly the same within the observational errors, indicative of chemical homogeneity in the primary and secondary sources of HCO⁺ and HNC.

The mass of the secondary source can be estimated assuming that the line intensity ratio between the primary and secondary line components, $s \sim 0.05$, is indicative of the local production rate Q_{ss} of the observed species, i.e., $Q_{\text{ss}} \sim sQ_{\text{ps}}$. For a monolithic spherical fragment, $r_{\text{ss}} \sim s^{1/2}r_n$ and $m_{\text{ss}} \sim s^{3/2}m_n$, where the mass of the nucleus $m_n \sim 10^{16}$ kg. For a source that is a debris field of small grains, the surface area-to-mass ratio for a grain relative to that for the comet nucleus scales as $(r_n/r_g)^{-1}$ (Harris et al. 1997). Therefore, very little total mass in the form of small grains is required to account for the secondary source HNC and HCO⁺ parent production. We estimate the total mass required for the secondary source to account for the observed line ratios in equations (14) and (15) to be roughly

$$m_{\text{ss}} \sim sm_n(r_n/r_g)^{-1} \sim 10^3 \text{ kg} \quad (16)$$

for 0.1 μm grains, where $r_n \sim 20$ km. The number of submicron-sized particles comprising the secondary source is then roughly $N \sim 3sm_{\text{ss}}(4\pi\rho_g r_g^3)^{-1} \sim 10^{20}$ grains for $\rho \sim 1000$ kg m⁻³.

5.3. Polymer Chemistry in the Secondary Source?

As mentioned previously, both HNC and HCO⁺ in the secondary source may arise directly from organic polymer material. As discussed by Rodgers & Charnley (2001), the HNC abundance in comet Lee cannot be reproduced by ion-molecule chemistry or by reactions of energetic H atoms with HCN, another possible route (Rodgers & Charnley 1998). Instead, these authors suggest that HNC arises from the photofragmentation of large organic HCN polymers in this comet, such as polyaminocyanomethylene.

HCO⁺ would require an oxygen-bearing polymer. Both CO and H₂CO have extended sources in several comets, including Halley and Hale-Bopp (Huebner et al. 1991; Wink et al. 1999). The proposed precursor for these two species is polyoxymethylene, a formaldehyde polymer with the formula $(-\text{CH}_2\text{O}-)_n$, or POM (Cottin et al. 2001). Because of photodestruction, this compound leads to H₂CO and CO, as well as CH₂ and CH (Huebner et al. 1991); HCO is another likely product. HCO⁺ could then be created by direct photoionization of HCO. Photoionization of this molecule has two possible sets of products, H+CO and HCO⁺, with a branching ratio of 2:1. Hence, the production of HCO⁺ from neutral HCO is a viable pathway. Quiet-Sun photofragmentation of H₂CO directly into HCO⁺ has a branching ratio of 1:1400 (Huebner et al. 1992), so it is also a possible pathway, depending on the relative abundances of HCO and H₂CO.

6. CONCLUSIONS

Observations of HCO⁺ toward comet Hale-Bopp conducted with the 12 m telescope indicate a large abundance of this species (~ 36 molecules cm⁻³) and the possibility of a secondary emission source composed of small fragments. This

secondary component was also observed at the same date in HNC emission. HCO^+ and HNC are products of ion-molecule chemistry in the primary source, although maps of these molecules show that HCO^+ is far more extended in its spatial distribution relative to the comet nucleus than HNC. HCO^+ is in fact present well beyond the collisionopause, suggesting that it is produced by reactants that are photodissociation products of H_2O , rather than H_2O itself. Calculations indicate that the process $\text{CO}^+ + \text{H}_2 \rightarrow \text{HCO}^+ + \text{H}$ is the major source of HCO^+ beyond the collisionopause, where almost all the water has been photodissociated. The secondary, high-velocity line components of HCO^+ and HNC can probably be explained by an ensemble of organic-rich, volatile grains accelerated by radiation pressure and, possibly, electrostatic forces. Destruc-

tion of polymer-like material in these grains may be creating both species. The variations in spatial distributions and the possible presence of secondary sources all indicate that the chemistry in comets, at least high production rate ones, is far more complex than the simple parent/daughter model. A wide variety of chemical and dynamical processes are obviously occurring on very short timescales that have only begun to be evaluated.

This research is supported by NASA through the NASA Astrobiology Institute under cooperative agreement CAN-02-OSS-02 issued through the Office of Space Science.

REFERENCES

- A'Hearn, M. F., Hoban, S., Birch, P. V., Bowers, C., Martin, R., & Klinglesmith, D. A. 1986, *Nature*, 324, 649
- Arpigny, C., Jehin, E., Manfroid, J., Hutsemekers, D., Schulz, R., Stuwe, J., Zucconi, J.-M., & Ilyin, I. 2003, *Science*, 301, 1522
- Blake, G. A., Qi, C., Hogerheijde, M. R., Gurwell, M., & Muhleman, D. 1999, *Nature*, 398, 213
- Bockelée-Morvan, D., et al. 2000, *A&A*, 353, 1101
- Boehnhardt, H. 2002, *Earth Moon Planets*, 89, 91
- Bouchez, A. H., Brown, M. E., Spinrad, H., & Misch, A. 1999, *Icarus*, 137, 62
- Charnley, S. B., Rodgers, S. D., Kuan, Y. J., & Huang, H. C. 2002, *Adv. Space Res.*, 30, 1419
- Cottin, H., Gazeau, M. C., Benilan, Y., & Raulin, F. 2001, *ApJ*, 556, 417
- Crovisier, J. 1987, *A&AS*, 68, 223
- Crovisier, J., & Bockelée-Morvan, D. 1999, *Space Sci. Rev.*, 90, 19
- Crovisier, J., & Encrenaz, T. 2000, *Comet Science: The Study of Remnants from the Birth of the Solar System* (transl. Stephen Lyle; Cambridge: Cambridge Univ. Press)
- Dello Russo, N., Mumma, M. J., DiSanti, M. A., Magee-Sauer, K., Novak, R., & Rettig, T. W. 2000, *Icarus*, 143, 324
- Desvoivres, E., et al. 1999, *MNRAS*, 303, 826
- DiSanti, M. A., Mumma, M. J., Dello Russo, N., Magee-Sauer, K., Novak, R., & Rettig, T. W. 1999, *Nature*, 399, 662
- Eberhardt, P. 1999, *Space Sci. Rev.*, 90, 45
- Gombosi, T., Hansen, K., DeZeeuw, D., Combi, M., & Powell, K. 1999, *Earth Moon Planets*, 79, 179
- Gunnarsson, M., et al. 2003, *A&A*, 402, 383
- Harmon, J. K., Campbell, D. B., Ostro, S. J., & Nolan, M. C. 1999, *Planet. Space Sci.*, 47, 1409
- Harris, W. M., Combi, M. R., Honeycutt, R. K., Mueller, B., & Schloerb, F. 1997, *Science*, 277, 676
- Hirota, T., Yamamoto, S., Kawaguchi, K., Sakamoto, A., & Ukita, N. 1999, *ApJ*, 520, 895
- Horanyi, M., & Mendis, A. 1991, in *Comets in the Post-Halley Era*, ed. R. L. Newburn, Jr., M. Neugebauer, & J. Rahe (Dordrecht: Kluwer), 1093
- Huebner, W. F., Boice, D. C., Schmidt, H. U., & Wegmann, R. 1991, in *Comets in the Post-Halley Era*, ed. R. L. Newburn, Jr., M. Neugebauer, & J. Rahe (Dordrecht: Kluwer), 907
- Huebner, W. F., Boice, D. C., & Sharp, C. M. 1987, *ApJ*, 320, L149
- Huebner, W. F., Keady, J. J., & Lyon, S. P. 1992, *Ap&SS*, 195, 1
- Huntress, W. T., McEwan, M. J., Karpas, Z., & Anicich, V. G. 1980, *ApJS*, 44, 481
- Ip, W.-H. 2003, *Celest. Mech. Dyn. Astron.*, 87, 197
- Ip, W.-H., & Jorda, L. 1998, *ApJ*, 496, L47
- Irvine, W. M., et al. 1998, *Faraday Discuss.*, 109, 475
- Jewitt, D. C., & Matthews, H. E. 1997, *AJ*, 113, 1145
- . 1999, *AJ*, 117, 1056
- Koch, A., van Hemert, M. C., & van Dishoeck, E. F. 1995, *J. Chem. Phys.*, 103, 7006
- Lederer, S. M., Campins, H., Osip, D. J., & Schleicher, D. G. 1999, *Earth Moon Planets*, 78, 131
- Le Teuff, Y. H., Millar, T. J., & Markwick, A. J. 2000, *A&AS*, 146, 157
- Lis, D. C., et al. 1999, *Earth Moon Planets*, 78, 13
- Lovell, A. J., Schloerb, F. P., Bergin, E. A., Dickens, J. E., De Vries, C. H., Senay, M. C., & Irvine, W. M. 1999, *Earth Moon Planets*, 77, 253
- Lovell, A. J., Schloerb, F. P., Dickens, J. E., De Vries, C. H., Senay, M. C., & Irvine, W. M. 1998, *ApJ*, 497, L117
- McCarthy, D., et al. 1999, *Earth Moon Planets*, 78, 243
- Mukai, T. 1986, *A&A*, 164, 397
- Narayanan, G., et al. 1997, *IAU Circ.*, 6591, 1
- Owens, A., Oosterbroek, T., Orr, A., Parmar, A. N., Schulz, R., & Tozzi, G. P. 1999, *Earth Moon Planets*, 77, 293
- Rodgers, S. D., Butner, H. M., Charnley, S. B., & Ehrenfreund, P. 2003, *Adv. Space Res.*, 31, 2577
- Rodgers, S. D., & Charnley, S. B. 1998, *ApJ*, 501, L227
- . 2001, *MNRAS*, 323, 84
- Schwarz, G., et al. 1999, *Earth Moon Planets*, 78, 189
- Sekanina, Z. 1982, in *Comets*, ed. L. L. Wilkening (Tucson: Univ. Arizona Press), 251
- . 1998a, *ApJ*, 494, L121
- . 1998b, *ApJ*, 509, L133
- Sekanina, Z., & Chodas, P. W. 2004, *ApJ*, 607, 620
- Sekanina, Z., & Farrell, J. A. 1980, *AJ*, 85, 1538
- Veal, J. M., et al. 1997, *IAU Circ.*, 6575, 1
- . 2000, *AJ*, 119, 1498
- Weaver, H. A., & Lamy, P. L. 1999, *Earth Moon Planets*, 79, 17
- Weaver, H. A., & Mumma, M. J. 1984, *ApJ*, 276, 782
- Weaver, H. A., et al. 2001, *Science*, 292, 1329
- Whipple, F. L. 1950, *ApJ*, 111, 375
- . 1999, *Planet. Space Sci.*, 47, 301
- Wink, J., et al. 1999, *Earth Moon Planets*, 78, 63
- Womack, M., Homich, A., Festou, M. C., Mangum, J., Uhl, W. T., & Stern, S. A. 1999, *Earth Moon Planets*, 77, 259
- Wright, M. C. H., et al. 1998, *AJ*, 116, 3018
- Wyckoff, S. 1982, in *Comets*, ed. L. L. Wilkening (Tucson: Univ. Arizona Press), 3
- Ziurys, L. M., Savage, C., Brewster, M. A., Apponi, A. J., Pesch, T. C., & Wyckoff, S. 1999, *ApJ*, 527, L67